PAPER

Multi-scale visualization and characterization of lignocellulosic plant cell wall deconstruction during thermochemical pretreatment†‡

Shishir P. S. Chundawat,*[ab] Bryon S. Donohoe,[c] Leonardo da Costa Sousa,[a] Thomas Elder,[d] Umesh P. Agarwal,[e] Fachuang Lu,[bf] John Ralph,[bf] Michael E. Himmel,[c] Venkatesh Balan[ab] and Bruce E. Dale[ab]

Deconstruction of lignocellulosic plant cell walls to fermentable sugars by thermochemical and/or biological means is impeded by several poorly understood ultrastructural and chemical barriers. A promising thermochemical pretreatment called ammonia fiber expansion (AFEX) overcomes the native recalcitrance of cell walls through subtle morphological and physicochemical changes that enhance cellulase accessibility without extracting lignin and hemicelluloses into separate liquid streams. Multi-scale visualization and characterization of *Zea mays* (*i.e.*, corn stover) cell walls were carried out by laser scanning confocal fluorescence microscopy (LSCM), Raman spectroscopy, atomic force microscopy (AFM), electron microscopy (SEM, TEM), nuclear magnetic resonance (NMR), and electron spectroscopy for chemical analysis (ESCA) to elucidate the mechanism of AFEX pretreatment. AFEX first dissolves, then extracts and, as the ammonia evaporates, redeposits cell wall decomposition products (*e.g.*, amides, arabinoxylan oligomers, lignin-based phenolics) on outer cell wall surfaces. As a result, nanoporous tunnel-like networks, as visualized by 3D-electron tomography, are formed within the cell walls. We propose that this highly porous structure greatly enhances enzyme accessibility to embedded cellulosic microfibrils. The shape, size (10 to 1000 nm), and spatial distribution of the pores depended on their location within the cell wall and the pretreatment conditions used. Exposed pore surface area per unit AFEX pretreated cell wall volume, estimated *via* TEM-tomogram image analysis, ranged between 0.005 and 0.05 nm^2 per nm^3. AFEX results in ultrastructural and physicochemical modifications within the cell wall that enhance enzymatic hydrolysis yield by 4–5 fold over that of untreated cell walls.

Background

The world is currently transitioning from a fossil fuel driven energy system to one that is supplied by a portfolio of more renewable and sustainable options.[1–3] The annual solar energy captured by non-food plant biomass ("lignocellulosic biomass"), such as grasses, woody materials, and agricultural residues (*e.g.*, corn stover), is nearly ten times that of the total energy used by humans.[4] Thus, lignocellulosic biomass will undoubtedly play an important and increasing role in our future energy portfolio, as recognized by the recent surge in government-supported bioenergy-related research worldwide.[5]

Inexpensive feedstocks and efficient conversion technologies are two key requirements to the successful commercialization of cellulosic biorefineries. Thermochemical pretreatment and enzymatic saccharification technologies are currently expensive and inefficient due to the recalcitrance of plant cell walls towards chemicals and enzymes.[6–8] Plant cell wall recalcitrance is a multi-scale phenomenon spanning several orders of magnitude encompassing both macroscopic and microscopic barriers (Fig. 1).[8] Both macroscopic-scale factors, such as tissue compositional heterogeneity and mass transfer limitations, and microscopic-scale factors, such as lignin-carbohydrate cross-linking

[a]Biomass Conversion Research Laboratory (BCRL), Chemical Engineering and Materials Science, Michigan State University, 3900 Collins Road, Suite 1045, Lansing, MI, 48910, USA. E-mail: chundawa@msu.edu; sousaleo@msu.edu; balan@msu.edu; bdale@egr.msu.edu
[b]DOE Great Lakes Bioenergy Research Center (GLBRC)
[c]Biosciences Center, National Renewable Energy Laboratory (NREL), Golden, CO, 80401, USA. E-mail: bryon.donohoe@nrel.gov; mike.himmel@nrel.gov
[d]USDA-Forest Service, Southern Research Station, Pineville, LA, 71360, USA. E-mail: telder@fs.fed.us

[e]USDA-Forest Service, Forest Products Laboratory, Madison, WI, 53726, USA. E-mail: uagarwal@fs.fed.us
[f]Department of Biochemistry, University of Wisconsin—Madison, WI, 53726, USA. E-mail: fachuanglu@wisc.edu; jralph@wisc.edu

This journal is © The Royal Society of Chemistry 2011

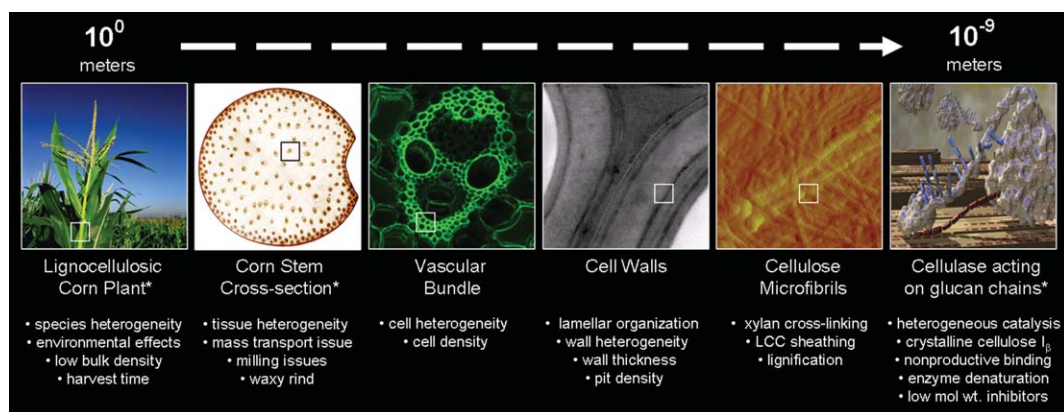*Energy Environ. Sci.*, 2011, **4**, 973–984 | 973

Fig. 1 Plant cell wall recalcitrance to enzymatic hydrolysis is a multi-length scale problem spanning several orders of magnitude. Asterisked (*) images courtesy of DOE/NREL.

and cellulose crystallinity, contribute synergistically to the recalcitrance of lignocellulosic biomass.[7]

Lignocellulosic plant cell walls are composed of crystalline cellulose nanofibrils embedded in an amorphous matrix of cross-linked lignin and hemicelluloses that impedes enzyme and microbial accessibility.[6] The primary goal of most chemical pretreatments is to overcome this lignin-hemicellulose barrier impeding enzymatic action, and in some cases to reduce cellulose crystallinity.[7] Thermochemical pretreatments, such as ammonia fiber expansion (AFEX) and dilute acid treatment, are two of the most promising methods to overcome the recalcitrance of native cell walls to enzymatic deconstruction.[9–12] Most pretreatments depolymerize and/or partly solublize hemicelluloses/lignin, extracting them into separate liquid streams, while leaving behind a solid cellulose-rich substrate that is more amenable to enzymatic hydrolysis.[12] However, the AFEX process appears to be somewhat unique in that it greatly enhances cell wall digestibility without removing any of the lignin or hemicelluloses into separate liquid streams.[11,13] AFEX also produces a substrate that is readily fermentable and does not require detoxification or external nutrient supplementation prior to fermentation.[14]

Though significant strides have been made recently in elucidating the chemical modifications within the cell wall following AFEX,[11,15] the ultrastructural effects and overall mechanism of AFEX pretreatment remain unknown. Examining the nanoscale architecture of pretreated cell walls in tandem with chemical, biochemical, and genetic characterization should provide insight into fundamental mechanisms that contribute to the native recalcitrance of cell walls.[16] This is especially true for the more recalcitrant lignified secondary cell walls which are poorly characterized compared to primary cell walls.[6,17,18] There is currently no systematic, multimodal, and integrated approach to developing models that explain the biochemical and ultrastructural organization of plant cell walls. Nor do we understand how this architecture is modified by thermochemical pretreatments from a holistic sense. Here, we examine AFEX pretreated cell walls using several multi-scale (i.e., micro- to nanometre scale) imaging and characterization techniques to develop multi-dimensional architectural models of ultrastructural modifications that result from pretreatment. These models provide insight into the fundamental mechanisms that influence the rate of biomass hydrolysis by enzymes. This work has immediate relevance to the biofuels arena, especially with the ongoing

Broader context

Cost-effective utilization of lignocellulosic biomass (e.g., corn stover, switchgrass) for production of fuels and chemicals is critical to the development of a bio-based economy. However, thermochemical pretreatments and enzymatic saccharification are currently expensive and inefficient due to the recalcitrance of lignocellulosic biomass towards its deconstruction to reactive biofuels or biochemical precursors. Examining the nano-scale architecture of pretreated lignocellulosic cell walls in tandem with chemical, biochemical and genetic characterization would provide insight into mechanisms that contribute to cell wall recalcitrance. Currently, there is no systematic, multimodal, and integrated approach to developing models that explain the biochemical and ultrastructural organization of plant cell walls, and more importantly, how this architecture is modified by thermochemical pretreatments to enhance the enzymatic digestibility. In this work, we examine ammonia (i.e., Ammonia Fiber Expansion or AFEX) pretreated cell walls using several imaging and characterization techniques to develop multi-dimensional architectural models of ultrastructural modifications that are a result of pretreatment. These models provide insight into the subtle physicochemical modifications that take place within plant cell walls during low-severity pretreatments and ultimately influence their enzymatic digestibility. This work has significant relevance to the biofuels arena with the on-going establishment of lignocellulosic biorefineries employing ammonia-based pretreatments.

This journal is © The Royal Society of Chemistry 2011

establishment of cellulosic biorefineries employing ammonia-based pretreatments.[19]

Results

Liquid–solid loading influences extent of pretreated cell wall disruption

Unlike AFEX, most pretreatments extract lignin (20 to 85% of the theoretical maximum) and/or hemicelluloses (30 to 80%) into separate liquid streams by applying 10 to 50 fold higher water loadings (*i.e.*, 3 to 20 g water per g dry biomass). There is a perceived need to extract these components in order to achieve an easily digestible substrate.[13,15,20–25] The impact of liquid–solid loading on corn stover cell wall morphology during AFEX was explored for two conditions with 15 min residence time at 130 °C: (A) L-AFEX (Low liquid loading) using 1 : 1 ammonia to biomass loading (w/w), 0.6 : 1 water to biomass loading (w/w); and (B) H-AFEX (High liquid loading) at 2 : 1 ammonia to biomass loading (w/w), 2 : 1 water to biomass loading (w/w). Since vascular bundle cells are known to be especially recalcitrant and contribute nearly 70 to 80% of the stem internode mass,[26] their cell walls were characterized in detail. Cell wall perimeter (L), wall-enclosed lumen area (A) and isoperimetric quotients ($Q = 4\pi A/L^2$) were determined to define the circularity (note: $Q = 1$ for a circle) of cell walls to estimate the severity of degradation as a function of cell type and pretreatment condition tested. Scanning electron micrographs (SEM) of L-AFEX pretreated material revealed no perceptible modification of internode cell walls, including epidermal cells, vascular bundles, parenchyma cells, or lignified sclerenchyma cells (Fig. 2 and S1-I‡). However, H-AFEX treatment resulted in complete disruption of parenchyma cells, collapse and aggregation of vascular bundles ('A', 'L' and 'Q' dropped by 74%, 48% and 6%, respectively, Fig. S1-II‡) and deposition of cell wall extractives on the outer cell walls and inner lumen spaces. The H-AFEX extractives deposited outside the cell walls were strongly stained by Safranin O dye, as indicated by confocal fluorescence imaging analysis (Fig. S1-III‡), suggesting that these deposits are enriched in lignin-derived phenolics. Glucan conversion after 24 h hydrolysis (15 FPU cellulase per g glucan loading) was marginally lower for H-AFEX (59 ± 9%) compared to L-AFEX (68 ± 8%).

Nano-sized extractives deposited on outer cell wall surfaces after AFEX

Atomic force microscopy (AFM; amplitude and phase) images were captured for secondary wall thickened vascular bundle cell surfaces (Fig. 2 and S2‡). Representative SEM and AFM images were taken from a collection of over 50 images each for untreated and L-AFEX treated corn stover cell walls at various magnifications. A fibrous network of cellulosic macrofibrils was typically seen for untreated walls along with occasional cytoplasmic remnants, crevices and cracks that formed part of the natural cell wall surface landscape.[27] The cellulose macrofibril width for never-dried untreated walls was 42 ± 3.4 nm ($n = 10$), which dropped to 23 ± 3.1 nm ($n = 10$) upon air-drying. Drying and extensive sample preparations (*i.e.*, extraction of residual hemicelluloses by alkali and other solvents) are known to modify the morphology of microfibrils.[27–29] The AFM tip adheres more strongly to hydrophilic areas that hence appear lighter in color (*i.e.*, greater change in phase). L-AFEX pretreated cell wall surfaces were found to be non-uniformly covered by irregularly shaped, hydrophilic deposits (20–1000 nm in width), unlike the hydrophobic lignin droplets seen on fiber surfaces after acidic pretreatments.[30,31] Surface roughness factor (RMS or root mean square; nm) was 2-fold greater for AFEX treated wall surfaces compared to untreated controls (Fig. S2-III‡). Untreated corn stover surfaces were predominantly hydrophobic (indicated by darker phase images). This was not the case for AFEX treated cell walls where a distinct phase contrast was visible. AFEX treated outer cell wall phase images had several lighter patches that corresponded to regions abundant in hydrophilic species.

Changes in pretreated cell wall architecture reveal the mechanism of AFEX

Inner cell wall ultrastructure was probed for untreated and AFEX treated corn stover by transmission electron microscopy
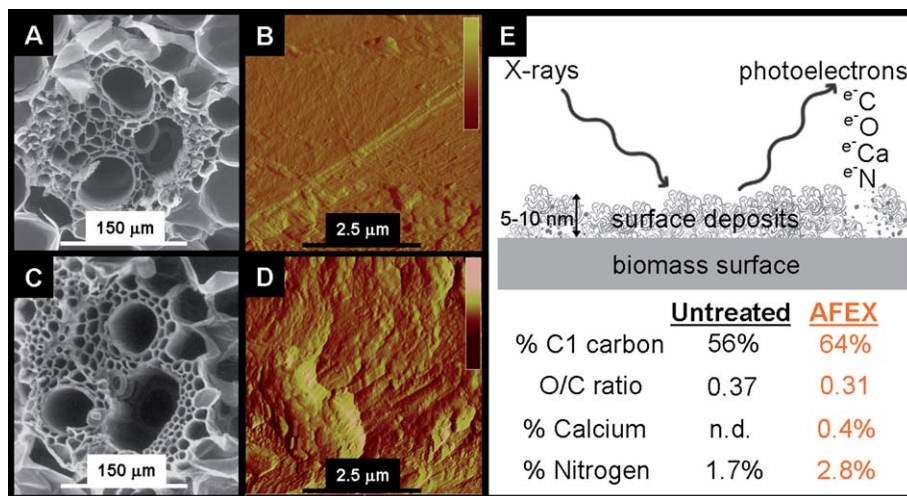

Fig. 2 SEM and AFM amplitude images for untreated (A and B) and L-AFEX (C and D) treated corn stover. ESCA-based surface atomic composition (E) of untreated and L-AFEX treated corn stover. Color legend (dark-light shades) for AFM images depicts the amplitude current scale (0–2.5 volts). n.d. stands for 'not detected'.

(TEM) (Fig. 3 and S3-I‡; Movies S4–S8‡). The compound middle lamella (CML) and secondary cell walls (S1–S3) are clearly visible in the untreated control. Regions of the cell wall that stained [with KMnO$_4$ and UO$_2$(CH$_3$COO)$_2$] black/dark grey are enriched in lignin,[9,32] whereas lighter grey regions are enriched in hemicelluloses and cellulose.[33] To study the effects of pretreatment on cell wall structure, the following AFEX reaction conditions were tested: (A) LA-AFEX (Low Ammonia loading) at 0.5 : 1 ammonia to biomass loading (w/w), 0.6 : 1 water to biomass loading (w/w), 15 min residence time at 130 °C; (B) L-AFEX (as before); (C) HAT-AFEX (High Ammonia loading and long residence Time) at 3 : 1 ammonia to biomass loading (w/w), 0.6 : 1 water to biomass loading (w/w), 45 min residence time at 130 °C; (D) Lt-AFEX (Low temperature) at 1 : 1 ammonia to biomass loading (w/w), 0.6 : 1 water to biomass loading (w/w), 15 min residence time at 70 °C; and (E) LW-AFEX (Low Water loading) at 1 : 1 ammonia to biomass loading (w/w), 0.05 : 1 water to biomass loading (w/w), 15 min residence time at 130 °C. Approximately, 3–5 different samples of each AFEX condition were sectioned and imaged by TEM. A total of 397 standard TEM images of ultrathin sections and 32 tomographic reconstructions from semi-thick sections (equivalent of 4580 standard images) were collected and visually inspected. The best representative examples for each AFEX condition were analyzed and quantified (with a minimum of 10 images analyzed to obtain quantitative data for each ultrastructural difference), some of which are presented here.

Large pores (10 to 500 nm in width) were formed within the CML after LA-AFEX due to the rapid decompression and volatilization of hot ammonia (i.e., no holes seen within Lt-AFEX CML). However, upon further increasing ammonia loading or reaction temperature (closer to the glass transition temperature of lignin, ~150 °C), the CML collapsed with its contents extruded into cell corners, pits and outer wall surfaces along with significant delamination/kinking of secondary cell walls. Randomly distributed, irregularly shaped extractive particles (20 to 200 nm in thickness) were found on the outer cell walls of L-AFEX validating the previous AFM findings. Immunolabeling revealed that these surface extractives were enriched in arabinoxylans (Fig. S3-II‡). Large ellipsoidal pores (semi-major and semi-minor axes lengths of 162 ± 47 nm and 73 ± 21 nm, respectively) were formed within the lumen-facing secondary walls for HAT-AFEX (Fig. S3-I-E and F‡). The eccentricity (0.88 ± 0.05) of the pores suggests that the lamellar orientation of the cellulosic microfibrils in the secondary cell walls forces anisotropic decompression of ammonia.[34] Also, liquid to gaseous phase decompression of ammonia results in deposition of extractables (derived from hemicelluloses and lignin) on the outer periphery of the pores for HAT-AFEX. We conclude that the explosive expansion of ammonia from the cell wall into the lumen space causes the cellulose microfibrils (4.1 ± 0.5 nm in diameter; Movie S6‡) to be "blown" outwards from the secondary cell walls. The elementary microfibrils are seen coated with a thin layer of lignin and/or hemicellulose rich residue (indicated by darker peripheral staining), supporting previous hypotheses regarding the organization of cellulose–hemicellulose within cell walls.[27] In the absence of water, the secondary wall is severely disrupted by anhydrous ammonia (Fig. S3-I-J and Movie S7‡), causing it to detach and resulting in the formation of dark stained, globular structures (128 ± 22 nm in diameter). Coalescence of inter-lamellar lignin packed between adjacent cellulosic fibrils (fibrils are typically separated by 15 to 70 nm[34]) forms these globular structures which are surrounded by a matrix of hemicelluloses and cellulose. Similarly sized lignified globular structures with a core–corona (lignin hydrophobic core and polysaccharide hydrophilic corona) suprastructure organization have been reported for wood derived lignin–carbohydrate complexes,[35,36] as well as for dilute-acid pretreated switchgrass.[37]
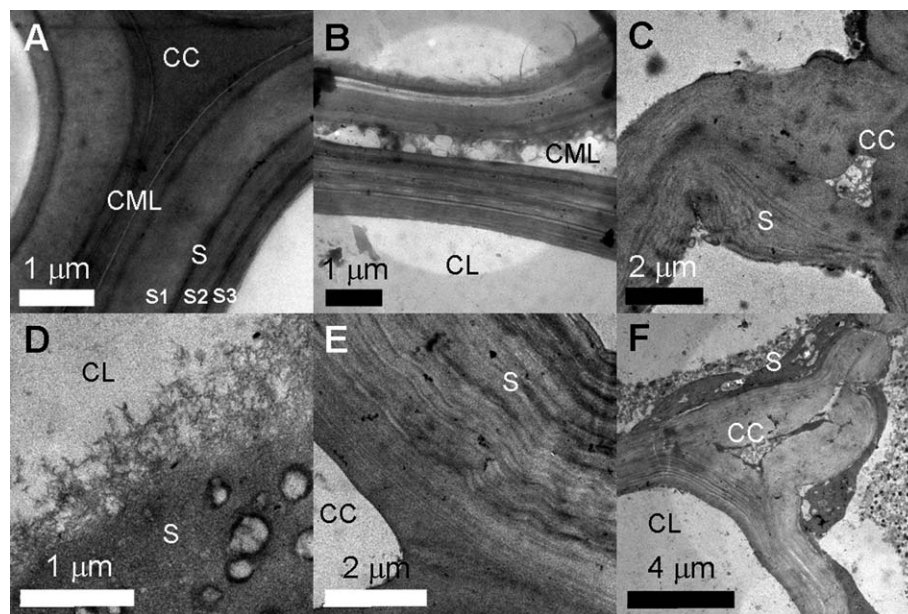

Fig. 3 TEM images depicting ultrastructure of cell walls before (A) and after AFEX for various pretreatment severities, namely; LA-AFEX (B), L-AFEX (C), HAT-AFEX (D), Lt-AFEX (E) and LW-AFEX (F). Cell corners (CC), cell lumen (CL), compound middle lamella (CML), and secondary wall layers (S) are labeled.

Nakashima and co-workers have shown deposition of 100–160 nm diameter lignin enriched spherical globules between cellulose microfibrils during lignification of secondary wall thickened tracheary elements in *Zinnia elegans*,[17] which draws close comparisons to the globular structures released from the S3 secondary cell walls during LW-AFEX.

3D-Tomograms (Movies S4–S8‡) were assembled from tilt-series TEM images and analyzed using the image segmentation and isosurface tools within the IMOD software package.[38,39] Porous spaces (*i.e.*, unstained regions) within pretreated cell walls were modeled by enclosing them with iso-surface mesh contours (Fig. 4) in order to compute accessible iso-surface area (nm^2) per unit volume (nm^3) of the cell wall (Table S9‡). Nearly 50–90% of the total porosity for LA-AFEX was within the CML and S1 secondary walls. However, with increased ammonia loading the outer secondary walls contribute significantly to the porosity with less than 15% contribution from the CML region. There were no discernible pores seen within untreated cell walls. Pores within untreated cell walls were not amenable to be measured using IMOD volume segmentation techniques as these pores are at the resolution limit to be distinguished from background noise. The advantage of TEM tomography is discerning the 3D nanoscale structural data within intact biological samples; however, one limitation is the 3D spatial resolution of ~5 nm and a reconstruction limitation known as the missing wedge that results in lower resolution in the Z axis than in $X–Y$ (Z axis resolution is 5–6 nm while $X–Y$ resolution is 1–2 nm).[38,40] This therefore limits discerning of pores within untreated cell walls, *via* conventional tomography, that are known to be typically much smaller than 5 nm.[41] However, the advantage of this technique is to discern the relative distribution of pores within pretreated cell walls as a function of pretreatment severity. The total porosity for L-AFEX, based on its tomogram analysis by IMOD, was approximately 23 $m^2 g^{-1}$ cell wall which is within the range (20–100 $m^2 g^{-1}$) reported for pretreated cell walls.[42,43]

BET (Brunauer–Emmett–Teller) nitrogen physisorption analysis underestimated the surface area by 10 to 15 fold in L-AFEX, confirming previous reports that BET is an inadequate technique for such materials.[43] It is likely that pores within plant cell walls collapse during sample preparation or BET analysis that reduces overall nitrogen accessible porosity. There have been reports in the inconsistency of the nitrogen adsorption regime in micropores in the presence of mesopores that make it theoretically difficult to accurately characterize pore structures.[44] This is especially a problem if the mouth of the pore is much smaller than the bulk of the pore volume (*i.e.*, an ink bottle shape with a small mouth opening). This could result in nitrogen condensation at the pore mouth without much penetration into the pore, which would result in an underestimation of the total porosity. TEM tomography has shown that this type of narrow mouth, ink bottle pore architecture is quite common within pretreated cell walls (Fig. 4) and could explain the discrepancy seen in the results from BET analysis compared to TEM based porosity. However, TEM based pore analysis is limited by the staining ability of the chemicals used to visually differentiate pores from the cell wall background which could create some bias in the results as well.

Relocalized, surface deposited 'extractives' are rich in lignin, hemicelluloses and cell wall decomposition products

Elemental chemical composition for outer wall surfaces was obtained by electron spectroscopy for chemical analysis (ESCA) (Fig. 2). There was a significant reduction in the surface oxygen (O) to carbon (C) content after AFEX (30% drop in O/C atomic ratio) along with a corresponding increase in C1/C2 carbon ratio (Fig. S10-I‡). This suggests that AFEX treated cell wall surfaces were enriched in reduced-oxygen components (*e.g.*, lignin) along with a concomitant decrease in oxygen-rich compounds (*e.g.*, cellulose). Calcium and nitrogen content of wall surfaces
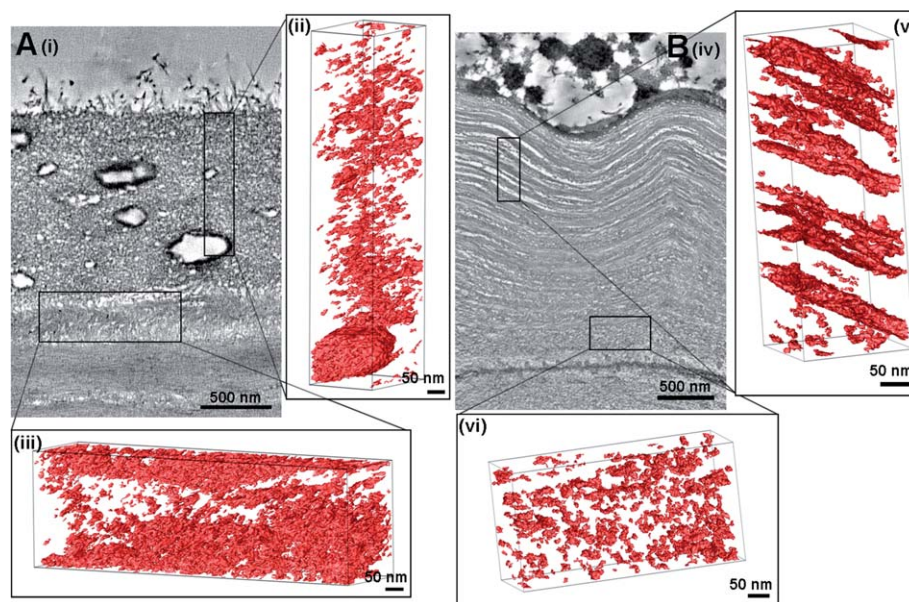

Fig. 4 Modeling porous regions within HAT-AFEX (A: i–iii) and LW-AFEX (B: iv–vi) pretreated cell walls using 3D-TEM tomograms. Isosurface mesh enclosing pore spaces within a HAT-AFEX cell wall (i) sub-volume of S3 layer (ii) and S2 delamination zone (iii). Isosurface mesh enclosing pore spaces within a LW-AFEX cell wall (iv) sub-volume of the S2 layer (v) and S1 layer (vi).

increased significantly after AFEX. Calcium is bound to pectic polysaccharides found in the middle lamella and primary cell walls.[45] The compound middle lamella is known to have high solubility in alkaline solutions[46] and can be delignified with comparative ease.[47] This explains the increased abundance of calcium on outer wall surfaces after L-AFEX. There was no significant difference in the elemental composition upon varying the angle of emission between 15° and 75° suggesting that the average thickness of the extractives surface layer was greater than 10 nm. Extracting the cell walls with water reduced the drop in O/C ratio to 10% (compared to untreated stover) indicating that a significant portion of the surface deposits are hydrophilic in nature (Fig. S10-I‡). The water extract was abundant in phenolics, further suggesting that these compounds are partly responsible for the reduction in the O/C ratio. The water soluble extractives from AFEX treated cell walls are also abundant in low and high molecular weight hemicellulose oligomers, lignin aromatics and decomposition products formed during pretreatment (*e.g.*, acetamide, phenolic amides, carboxylic acids).[11]

After L-AFEX pretreatment, approximately 50% of the lignin in corn stover is rendered soluble in a 9 : 1 acetone : water solution, a solvent suitable for lignin solubilization. After lyophilizing and water washing (to remove soluble sugars and other components), the residue was found to be composed mostly of lignin which represented over half of the lignin found in the original material. Preliminary characterization by NMR showed this to be a somewhat syringyl-enriched syringyl–guaiacyl lignin in which the lignin polymer had not been significantly degraded (Fig. S10-II‡). The extract also contained *p*-coumaroyl and feruloyl amides formed during ammonolytic cleavage of *p*-coumarate and ferulate esters in the cell wall. NMR revealed that most of the *p*-coumarate esters were cleaved during AFEX and only ∼10 to 15% of the *p*-coumarate remained as intact esters in the extractable lignin. The postulated removal of lignin during AFEX is further supported by the FT-Raman analysis of untreated and L-AFEX treated stover (Fig. S11‡). The residual lignin peaks (at 1600 and 1635 cm^{-1}) are about 3 times higher in the control sample indicating that AFEX treatment caused ultrastructural modifications that led to more lignin removal during the acid chlorite sample treatment step (see methods section for details on sample preparation prior to Raman spectroscopy). Additionally, Raman analysis based on the 1170 cm^{-1} cinnamoyl ester band indicated that the residual lignin had significantly lower (71% lower) ferulate and *p*-coumarate groups.

Enzymatic accessibility to crystalline cellulose increases after AFEX

Enzymatic hydrolysis (for 24 h) was carried out on untreated and L-AFEX corn stover using various combinations of purified and crude *Trichoderma reesei* cellulases (Fig. 5). Cellobiose was the major hydrolysis product for L-AFEX upon addition of exocellulases (Cel7A or CBH I and Cel6A or CBH II) as compared to untreated corn stover which resulted in glucose as the major product. Treatment with the endocellulase (Cel7B or EG I) resulted in glucose as a major product for untreated cell walls. Control experiments with isolated microcrystalline cellulose (Avicel) revealed that the ratio of cellobiose to glucose released by Cel7A and Cel7B was 11.5 ± 4.8 and 3.4 ± 0.6, respectively. These results indicate that AFEX enhances the accessibility of
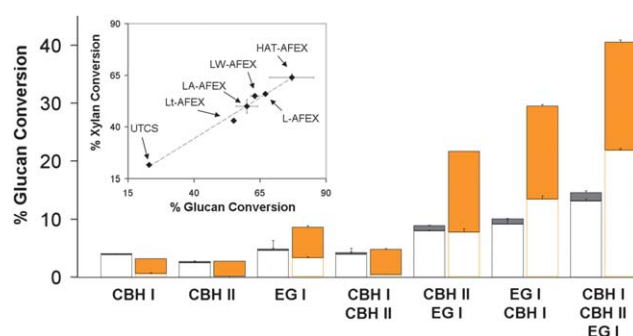

Fig. 5 Glucan hydrolysis yield (24 h) of untreated (UTCS; left bar in grey) and L-AFEX treated corn stover (right bar in orange) by purified *Trichoderma reesei* cellulases. Empty and filled bars depict glucose and cellobiose yields, respectively. Inset depicts glucan and xylan hydrolysis yields (15 FPU Spezyme CP per g glucan loading) for corn stover treated with various AFEX severities.

crystalline cellulose microfibrils to exo-cellulases. Enzymatic digestibility (for 24 h) using a crude cellulases broth (Spezyme CP/Novo 188) to saccharify corn stover pretreated under five different AFEX severities (*e.g.*, L-AFEX) revealed that glucan and xylan conversions were closely correlated (Fig. 5). Increasing cellulose accessibility during AFEX, as evidenced by TEM analysis, enhances both glucan and xylan digestibility.

Discussion

Several literature reports have suggested that the physical removal of lignin and hemicelluloses from plant cell walls into separate liquid phases is necessary to enhance cellulose accessibility to hydrolytic enzymes. Recent findings, including this current work, indicate to the contrary that subtle changes in the inner cell wall localization of the lignin and hemicellulose components during mild pretreatments (like AFEX) can also enhance cellulose accessibility.[9,31] Also, not removing cell wall extractables and other nutrients (*e.g.*, sugars, minerals, proteins, amides) can significantly improve hydrolyzate fermentability, obviating the need for exogenous nutrient supplementation.[11,14,48] Lignin and hemicellulose extraction from within cell walls to outer cell wall surfaces during AFEX (at low liquid–solid loadings) is expected to be diffusion-limited.[49] Surprisingly, there was no improvement of the overall cellulose hydrolysis yield for corn stover that was AFEX pretreated at higher water loadings, possibly due to inhibition of enzymes by the greater density of surface exposed lignin for H-AFEX *versus* L-AFEX.[50] Similar hydrolysis results have been reported for ammonia recycle percolation (ARP), an aqueous ammonia pretreatment technique using much higher water loadings than AFEX.[20] Increased ammonia and water usage during pretreatment would necessitate significant capital investment in solvent recovery.[19,51–53] Thus it is crucial to gain a fundamental understanding of the ultrastructural and physicochemical changes occurring within the cell wall during low liquid-to-solid loading ammonia-based pretreatments and to better understand how these changes enhance enzymatic digestibility and microbial fermentability.

Until recently, physicochemical and ultrastructural effects of ammonia-based pretreatments on plant cell walls were poorly understood compared to their acidic counterparts.[11] O'Connor

showed that ammonia-based pulping of aspen wood results in kinking and curling of treated cell walls with fiber separation noted along the middle lamella and outer secondary cell walls.[54] Weimer and colleagues also noticed surface deposition of a nebulously shaped layer after supercritical ammonia treatment of hardwoods.[55] These findings are consistent with the current model for the mechanism of AFEX (Fig. 6). Ammonia penetrates the cell walls from the outer walls facing the lumen and middle lamella. Here, in the presence of water a series of ammonolytic and hydrolytic reactions cleave various ester linkages (hemicellulose acetates, *p*-coumarates, ferulates, and diferulates acylating hemicelluloses, and lignin *p*-coumarates) resulting in the formation of corresponding amides and acids.[11] Cleavage of lignin–hemicellulose ester linkages, including the important cross-links mediated by ferulates, facilitates the solubilization and removal of hemicellulose oligomers and other extractables to outer cell wall surfaces, cell corners and pits, exposing the embedded cellulose microfibrils. These extractives are rich in arabinoxylan oligomers, amides, minerals and cell wall degradation products released/formed during AFEX.[11] At the end of pretreatment, the rapid pressure release results in convective transport of ammonia–water and cell wall extractables towards the cell lumen and cell corners (through the middle lamella). The expansive decompression of ammonia at the wall periphery results in the formation of large pores in the middle lamella and outer secondary cell walls. The sizes of the pores seen within the treated cell walls are typically larger than 10 nm, which would greatly facilitate the accessibility of cellulases (note: Cel7A from *Trichoderma reesei* has a radius of gyration ∼5 nm and a maximum length ∼12 nm). This fact does much to explain the increased activity of cellulases on crystalline cellulose within pretreated cell walls (Fig. 5). The TEM tomograms highlight not only the increased porosity, but also the extensive interconnectedness of the pore network created by AFEX pretreatment. Indeed, not all pore networks are directly connected to cell wall surfaces, but this is not necessarily needed in order to enhance enzyme accessibility. Previous work has shown that enzymes readily access cell wall surfaces, cell corners, middle lamella, cell pits, and delamination surfaces created during dilute-acid pretreatment.[56] Also, the interconnectedness indicates that once a pore surface is reached, the enzymes should immediately gain access to an extensive new surface. However, studying the change in cell wall pore morphology *in situ* during the course of enzymatic hydrolysis is a challenge that would further elucidate the role of wall porosity on enzyme diffusion (*e.g.*, influence of pore tortuosity), non-specific protein binding (*e.g.*, to lignin lining the outer periphery of pores) and overall hydrolysis kinetics. Fungi and microbes typically attack plant cell walls from their cell lumena or middle lamella regions due to easier physical accessibility or possibly abundance of nutrients (*e.g.*, sugars, proteins). Hydrolytic enzymes and pretreatment chemicals probably gain access to cell walls from these regions first, as we notice that the extent of cell wall deconstruction during AFEX is relatively more severe for CML and S3 regions. Similar effects have been noted for cellulase accessibility to acid treated corn stover cell walls.[9,56] Interestingly, kraft pulping of spruce wood fibers has also been shown to cause increased pore and matrix lamella width in fiber walls closest to the middle lamella that gradually decrease in size towards the cell lumen.[57] The relative contribution of mass

transfer (*e.g.*, S3 *versus* S2 sub-layer accessibility to chemicals and extraction of lignin/hemicellulose from these layers) and cell wall composition (*e.g.*, LCC linkage frequency in S3 *versus* CML and/or lignin composition influencing lignin–hemicellulose removal) influencing the physicochemical impacts of thermochemical pretreatments is currently unclear and should be explored in the future to fundamentally understand the rate-limiting steps to lignocellulose deconstruction.[8]

It is clear that the amount of extractables removed is related to the amount of ammonia–water used during pretreatment. In the absence of water, the outer secondary cell walls collapse completely due to coalescence of lignin, resulting in significant kinking of the cell walls. Interestingly, extensive degradation of the outer walls did not increase the glucan digestibility compared to L-AFEX. This observation reinforces the point that extensive decomposition of the cell wall during AFEX pretreatment (and possibly other thermochemical pretreatments) does not always result in improved digestibility. On the contrary, the lignin globules coalescing during LW-AFEX, similarly to lignin globules reported from acid treated corn stover[30] and synthetic dehydrogenation lignin polymer based nano-aggregates,[35] are likely responsible for inhibiting hydrolytic enzymes. Increasing the cell wall porosity without extensively extracting lignin and hemicelluloses should prevent collapse and aggregation of cellulose microfibrils that ultimately reduces pretreatment effectiveness.[9,37]

Lignins cannot be solvent-extracted from corn stover to any significant extent except when it is finely milled (*i.e.*, ball-milled). However, after AFEX, a significant portion (∼50%, w/w) of the lignin can be readily extracted by acetone : water mixtures. Preliminary NMR examination shows the core lignin polymer to be intact after AFEX and similar in chemical structure to native lignin. *p*-Coumarate esters were ammonolyzed during AFEX, and ferulate–polysaccharide esters in the cell wall were also cleaved. Thus, as shown in (Fig. S10-II‡), only about 10% of the *p*-coumarate esters remain after AFEX, with most being converted to *p*-coumaroyl amides. Although ferulate esters are not seen in the lignin isolated from corn stover (because they are associated with polysaccharides and do not extract into this fraction), their presence is readily noted in the solvent-soluble fraction after AFEX.[11] Clearly, significant cleavage of esters, producing amides, is a major cell-wall-disrupting reaction occurring during AFEX pretreatment of grasses. Cleavage of diferulate linkages (which cross-link polysaccharides), and lignin–ferulate and lignin–diferulate linkages (which cross-link polysaccharides to lignin), and other ester linkages, during AFEX is expected to facilitate removal of lignins and increase enzyme accessibility to the polysaccharides.[11] Genetically engineering ester linkages into the backbone of the lignin polymer,[58,59] augmenting the ether- and carbon–carbon-linked structures should further facilitate the efficiency of delocalizing lignin and hemicelluloses during AFEX.

There was no significant transformation of the native cellulose crystal structure to other crystalline states (*e.g.*, cellulose III$_I$) during conventional L-AFEX (Fig. S11‡), as evidenced by no significant change in the ratio of 350 and 380 cm^{-1} Raman band intensities. This is expected since water likely prevents the transition of cellulose I to III$_I$ by competing with ammonia's ability to intercalate and disrupt the elementary microfibril hydrogen-bonded network.[60] Pretreatment of isolated cellulose under
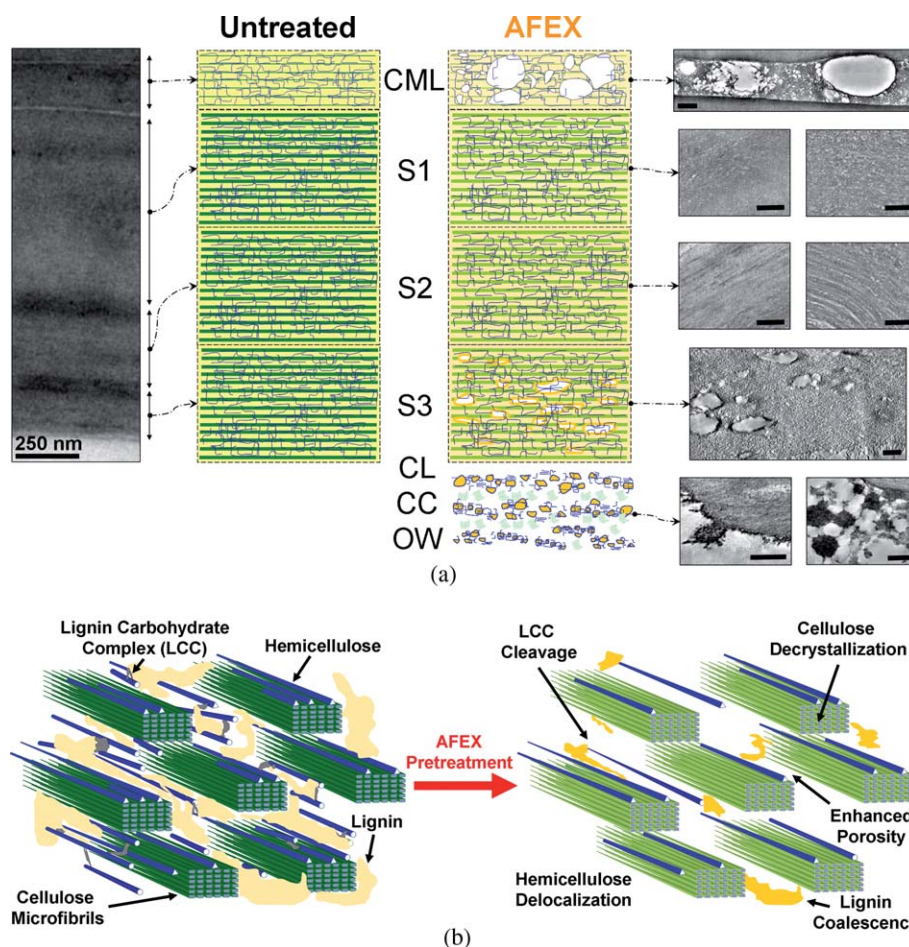
Fig. 6 Schematic models for lignocellulosic cell walls depicting overall microscale (a) and nanoscale (b) ultrastructural modifications as a result of ammonia based pretreatments. Pretreatment results in cleavage of lignin–carbohydrate complex linkages between non-core lignin phenolics and hemicellulose side-chains that allows removal/redeposition of cell wall decomposition products onto outer wall surfaces and hence results in increased wall porosity (white spaces). Different components of the cell wall depicted are: cellulose (green lines), hemicelluloses (blue strings), lignin (yellow matrix), cell corners (CC), cell lumen (CL), outer wall surfaces (OW), compound middle lamella (CML), secondary wall layers (S1, S2, S3). Scale bar is 250 nm.

L-AFEX conditions resulted in no significant change in its crystallinity or enzymatic digestibility.[61] However, in the absence of water during AFEX there was some partial conversion to cellulose III$_I$ (Fig. S11‡). These results suggest that conventional L-AFEX improves the digestibility of plant cell walls by enhancing crystalline cellulose accessibility to cellulases by removal of lignin and hemicelluloses from their close association with the cellulose without any significant alteration of the cellulose crystal structure. Future work will focus on altering the crystalline state of cellulose (*i.e.*, to produce cellulose III$_I$ during AFEX) in addition to the physicochemical changes currently seen during conventional AFEX to exploit the improved digestibility reported for cellulose III$_I$.[61,62]

Conclusion

Plants have evolved complex biochemical strategies buttressed by a rigid, recalcitrant cell wall to the counter attack by fungi and microbes. Despite the extensive biochemical and genetic studies that have been carried out to unveil the structure and function of cell walls, there have been very few multi-scale imaging and

modeling studies to complement that effort. In this paper, we report the first multi-modal approach to image and characterize monocot (*i.e.*, *Zea mays*) cell walls before and after thermochemical pretreatment (*i.e.*, AFEX). Most thermochemical pretreatments strip out lignin and hemicellulose along with nutrients (which might prove valuable for downstream fermentation) using high liquid to solid solvent loadings during pretreatment to improve enzymatic digestibility. On the contrary, conventional AFEX pretreatment employing much lower solvent loadings improves polysaccharide digestibility *via* cleaving lignin–carbohydrate ester linkages, partially solubilizing cell wall extractables and relocating these extractables to cell wall surfaces, thereby creating porous, interconnected tunnel-like networks that are much more accessible to enzymes. AFEX pretreatment was found to significantly modify the middle lamella and outer secondary cell walls regions, suggesting that mass transfer considerations for cell wall extractables removal are a major barrier to its effective deconstruction during pretreatment. However, there still remains much to be learned about these phenomena. These studies reinforce the fact that extensive decomposition of cell walls during pretreatment is not

a necessary criterion to improve biomass conversion to fermentable sugars. Future advances in the cell wall genetic engineering to overcome the native recalcitrance to deconstruction suited for low thermochemical severity pretreatments such as AFEX are expected to further reduce the cost of plant-derived fuels and chemicals.

Materials and methods

Biomass source

Fresh whole corn plants were harvested from MSU farms and used for certain microscopy experiments (*e.g.*, AFM, SEM, and LSCM). MSU corn stems were hand sectioned using a razor blade into thin slices (slice thickness ranging from 100 μm to 1 mm) and air-dried (to the desired moisture level) in a clean hood prior to AFEX treatment. Pre-milled corn stover (Pioneer hybrid seed variety 33A14 harvested in 2002 from the Kramer farm in Wray/Colorado for CAFI projects), passed through a 10 mm screen, was provided by the National Renewable Energy Laboratory (NREL). NREL corn stover was used for TEM, ESCA and enzymatic hydrolysis experiments. The pretreated biomass was stored in the fridge at 4 °C prior to being characterized.

AFEX pretreatment

AFEX pretreatment on MSU corn stem cross-sections was carried out in a 22 mL bench-top reactor (316 SS, PARR Instrument Co, IL). The vessel was loaded with the feedstock at the appropriate moisture content (0%, 60% or 200%, dwb). The reactor was clamped shut and the required amount of ammonia (1 : 1 or 3 : 1 ammonia to biomass loading, w/w) was injected using a pre-weighed ammonia delivery vessel. The reactor was heated using a custom made aluminium block on a hot plate and maintained at the desired temperature (within ±10 °C) for the necessary residence time. At the end of the residence time, the pressure was explosively released. The biomass was removed from the reactor and left in the hood overnight to remove the residual ammonia. AFEX pretreatment on NREL corn stover was carried out in a 2 L Parr reactor as described previously.[11] Crystalline cellulose III control was prepared using cotton linter derived cellulose (Sigma, St Louis, MO) based on previously published protocol.[60]

Scanning electron microscopy (SEM)

SEM was carried out on a JEOL (Japan Electron Optics Laboratories) 6400V SEM with a LaB6 emitter. Biomass samples were gold sputter coated without critical point drying (CPD), to avoid possible extraction of AFEX surface deposits during CPD, and imaged at accelerating voltages between 10 and 20 kV to prevent electron beam induced damage to the specimens. Cell wall lumen perimeter and enclosed area were calculated using Zeiss LSM Image Browser (Version 3.0, Carl Zeiss International, Jena, Germany).

Laser scanning confocal fluorescence microscopy (LSCM)

Untreated and AFEX pretreated MSU corn stems sections (slice thickness ranging from 100 μm to 1 mm) were stained with 1% Safranin O (Sigma, St Louis, MO) in distilled water for 15 min and observed using a Zeiss Pascal LSCM. Excitation from a 543 nm laser and emission passing through a long pass (LP) 560 nm filter was used for observing fluorescence. Sections of the tissue were also observed for auto-fluorescence without staining. Stacks of confocal optical sections were taken throughout the *z*-depth of the observed plant stem section. Several individual cross-sections were observed and extended focus images of the stacks were compiled using the maximum intensity algorithm software (LSM 5 Pascal Version 3, Carl Zeiss International, Jena, Germany).

Atomic force microscopy (AFM)

AFM imaging was conducted using a Dimension Nanoscope 3100 Scanning Probe Microscope (Digital Instruments) with a Nanoscope IIIa controller. Both amplitude and phase images were collected simultaneously in tapping mode (in air) with an MPP-11100, etched silicon probe with a nominal frequency of 300 kHz and a nominal spring constant of 40 N m^{-1}. Untreated cell walls were not air-dried prior to imaging (moisture content >50%, w/w) while pretreated cell walls were air-dried to remove the residual ammonia prior to imaging. RMS roughness factors were estimated after image flattening and plane fitting of the height images using the software that came with the instrument. The width of the cell wall microfibrils and AFEX deposits were calculated using Zeiss LSM Image Browser (Version 3.0, Carl Zeiss International, Jena, Germany).

Transmission electron microscopy (TEM) and 3D-TEM-tomography

Corn stover samples were processed using the microwave Electron Microscopy (EM) processing methodology.[9] Biomass was fixed twice for 6 min (2 min on, 2 min off, 2 min on) in 2.5% glutaraldehyde solution buffered in 0.1 M sodium cacodylate buffer (EMS, Hatfield, PS) under vacuum. Dehydration was carried out in a graded ethanol series for 1 min each (15%, 30%, 60%, 90%, twice for 100% ethanol). Samples were infiltrated with LR White (or Epon) resin in the microwave under vacuum and incubated overnight at room temperature with increasing concentrations of the resin (15%, 30%, 60%, 90%, thrice for 100% resin, diluted in ethanol). Samples were then transferred to gelatin capsules and the resin was polymerized by heating to 60 °C overnight. LR White embedded samples were sectioned to ~100 to 250 nm with a Diatome diamond knife on a Leica EM UTC ultramicrotome (Leica, Wetzlar, Germany). The sectioned samples were collected on Formvar coated copper or nickel slot grids (SPI Supplies, West Chester, PA). Grids were post-stained for 6 min with 2% aqueous uranyl acetate. The grids were also stained with 1% KMnO$_4$ for 10 min to selectively stain for lignin. Images were taken with a Gatan UltraScan 1000 camera (Gatan, Pleasanton, CA) on a FEI Tecnai G220 Twin 200 kV LaB6 TEM (FEI, Hilsboro, OR). Tomograms were created by capturing dual-axis ± 60–65° tilt series using Serial EM (http://bio3d. colorado.edu/). Tomograms were constructed using an *R*-weighted back projection algorithm within the IMOD software package (http://bio3d.colorado.edu/). Single-axis tomograms were then combined to yield dual-axis tomograms using

a warping algorithm within IMOD.[40] Tomograms were displayed and analyzed using the IMOD software package.[38]

Porous spaces (*i.e.*, unstained regions) within the pretreated cell walls were modeled by enclosing them using iso-surface mesh contours based on an optimum threshold value (ranges 130–170). One representative tomogram per AFEX condition was analyzed by IMOD to determine the porosity (tomograms are provided as ESI‡) within different regions within the cell wall as highlighted in Table S9‡. The tomograms were analyzed without binning the voxels intensities; however, to generate the iso-surfaces the image bin and smooth values were set between 3–4 and 10–15, respectively. The boxes enclosing the iso-surfaces typically ranged in *x*–*y* dimensions between 100 and 500 nm, while the *z*-scale thickness was typically 80–150 nm. Each pixel is 1 nm wide in the *x*–*y* plane, while it was assumed to be 1 nm in the *z*-direction (within the depth of the sample tomogram, assuming no beam-induced specimen thinning). Surface areas of iso-surfaces enclosing porous regions within a defined volume of the cell wall were obtained using the IMOD model. Total porosity within the cell wall was estimated by computing the fractional surface area to volume contributed by each region within the cell wall tomogram. The relative fractional thicknesses of the various regions within the cell wall (*i.e.* CML, S1, S2, S3, S1/S2/S3 delamination zones) were calculated based on the size of the congruous porous regions. Assuming the density of the cell wall to be uniform (*i.e.*, 1 gram of cell wall occupies 1 cm³ volume) the surface area of the porous regions per gram of biomass was computed.

Immuno-electron microscopy (IEM)

Anti-arabinoxylan LM-11 antibody was obtained from PlantProbes (Leeds, UK). The epitope for LM-11 has four xylose residues that are able to accommodate un-substituted and substituted xylan backbones.[63] For anti-xylan immuno-EM, sample grids were placed on 15 µL drops of 1.5% BSA (bovine serum albumin) in 1× PBS–0.1% Tween (PBST) for 30 min, blotted, then directly placed on 15 µL drops of respective primary antibodies diluted 1 : 10 in 1% BSA–PBST for 90 min. Following 3 × 1 min rinses, the grids were then placed on 15 µL drops of anti-rat (IgG) secondary antibody conjugated to a 15 nm gold particle (British BioCell, Ted Pella) diluted 1 : 100 in PBST. Samples were then rinsed 3 × 1 min with PBST and again in H_2O. The grids were post-stained with uranyl acetate and $KMnO_4$ for better contrast.

Nitrogen physisorption analysis

The Brunauer-Emmett-Teller (BET) surface area and pore size distribution were measured by nitrogen adsorption at 77 K using a Micromeritics ASAP 2700 instrument. At least 2–3 g of sample was used for each run and were degassed at 60 °C overnight prior to analysis.

Electron spectroscopy for chemical analysis (ESCA)

Surface chemical characterization was carried out using a Physical Electronics PHI5400 ESCA electron spectrometer equipped with a non-monochromatic Mg Kα (15 V, 300 W) X-ray source as described previously.[50] All spectra were typically collected at an optimal take-off-angle (TOA) of 45° for a 250 × 250 square

micron area. Some measurements were conducted at 15° and 75° to determine the thickness of surface extractives. Peak intensities were determined by peak area integration. Curve fitting to the carbon (1s orbital), oxygen (1s orbital), calcium (2p orbital) and nitrogen (1s orbital) peaks was carried out with a Lorentzian–Gaussian curve-fitting program. The carbon (C1s) signal was deconvoluted (within ±0.3 eV) into C1 (284.7 eV), C2 (286.4 eV), C3 (288.1 eV) and C4 (289.8 eV) signals. Samples were milled to <200 µm before AFEX. Some samples were extracted with hot water, as described previously,[11] prior to analysis.

Raman spectroscopy

Raman spectra were obtained using a near-IR FT-Raman spectrometer (RFS-100 Bruker Instruments Inc., Billerica, MA). The spectrometer was equipped with a 1000 mW 1064 nm continuous wave diode Nd : YAG laser, along with a liquid nitrogen cooled germanium detector. Samples were pressed into the aluminium wells and spectra were acquired using a 600 mW laser; 1024 scans were accumulated for each spectrum. Raman spectra were normalized based on the 1096 cm⁻¹ band of cellulose to allow comparison between samples. In order to obtain Raman spectra with minimum fluorescence interference, samples were delignified using acid chlorite and then bleached with sodium borohydride prior to analysis. The treatment method was as follows. To approximately 0.1 g substrate, about 10 mL of water was added. About 0.1 g of sodium chlorite was dissolved in to the water, continuously stirring the suspension, followed by adding a drop of acetic acid. The sample was then placed into a 60–70 °C water bath for 90 min with continuous stirring. The sample was centrifuged, washed three times with water, twice with 95% ethanol and once with acetone. To approximately 0.1 g of the acid chlorite treated samples, about 10 mL of a 1% (w/w) solution of sodium borohydride was added. The reaction was allowed to proceed for two hours at room temperature with periodic stirring. Upon completion, the samples were centrifuged and the liquid decanted off. The treated samples were washed three times with water, twice with 95% ethanol and once with acetone. The extent of cellulose III formation, if any, was determined based on the relative peak intensity of 380 and 350 cm⁻¹ as reported previously.[64]

Nuclear magnetic resonance (NMR) spectroscopy

Preliminary characterization of extractable lignins by NMR, and comparison with isolated corn stover lignin, was carried out as follows. Isolated corn stover lignin was prepared by dioxane–water extraction of the ball-milled extractive-free corn stover as described previously.[65] The AFEX 'delocalized surface lignin' was isolated from extraction of unground AFEX-treated corn stover with 9 : 1 acetone : water (at room temperature), followed by lyophilization. The dried powder was water-washed (over a 5 µm nylon filter) to remove saccharides and other water-soluble compounds. Two-dimensional ¹³C–¹H-correlation (HSQC) spectra in 9 : 1 acetone-d₆ : D₂O were obtained on a Bruker Biospin (Billerica, MA) Avance 500 MHz spectrometer fitted with a cryogenically cooled 5 mm TCI gradient probe with inverse geometry (proton coils closest to the sample) as described elsewhere.[66]

Modified Prussian blue phenolics analysis

Total phenolic content of the water soluble cell wall extractives was measured using the modified Prussian blue method. A detailed protocol is provided elsewhere.[50,67]

Cellulase purification, enzymatic hydrolysis and compositional analysis

Protocols for cellobiohydrolase (Cel7A, Cel6A) and endoglucanase (Cel7B) purification from *Trichoderma reesei* enzyme broth, microplate based high-throughput enzymatic hydrolysis and hydrolyzate sugar analysis are provided elsewhere.[68,69]

Acknowledgements

References

1 B. D. Solomon, *Ann. N. Y. Acad. Sci.*, 2010, **1185**, 119–134.
2 L. R. Lynd, J. H. Cushman, R. J. Nichols and C. E. Wyman, *Science*, 1991, **251**, 1318–1323.
3 L. R. Lynd, M. S. Laser, D. Brandsby, B. E. Dale, B. H. Davison, R. Hamilton, M. Himmel, M. Keller, J. D. McMillan, J. Sheehan and C. E. Wyman, *Nat. Biotechnol.*, 2008, **26**, 169–172.
4 R. D. Perlack, L. L. Wright, A. Turhollow, R. L. Graham, B. Stokes and D. C. Erbach, Biomass as Feedstock for a Bioenergy and Bioproducts Industry: The Technical Feasibility of a Billion-Ton Annual Supply, Oak Ridge National Laboratory, United States Department of Energy, 2005, pp. 1–78 (DOE Accession #ADA436753).
5 E. Kintisch, *Science*, 2007, **316**, 1827c.
6 M. Himmel, S. Ding, D. Johnson, W. Adney, M. Nimlos, J. Brady and T. Foust, *Science*, 2007, **315**, 804–807.
7 L. da Costa Sousa, S. P. Chundawat, V. Balan and B. E. Dale, *Curr. Opin. Biotechnol.*, 2009, **20**, 339–347.
8 S. P. S. Chundawat, G. T. Beckham, M. Himmel and B. E. Dale, *Annu. Rev. Chem. Biomol. Eng.*, 2011, **2**, DOI: 10.1146/annurev-chembioeng-061010-114205.
9 B. Donohoe, S. Decker, M. Tucker, M. Himmel and T. Vinzant, *Biotechnol. Bioeng.*, 2008, **101**, 913–925.
10 R. Brunecky, T. B. Vinzant, S. E. Porter, B. S. Donohoe, D. K. Johnson and M. E. Himmel, *Biotechnol. Bioeng.*, 2009, **102**, 1537–1543.
11 S. P. S. Chundawat, R. Vismeh, L. Sharma, J. Humpula, L. Sousa, C. K. Chambliss, A. D. Jones, V. Balan and B. E. Dale, *Bioresour. Technol.*, 2010, **101**, 8429–8438.
12 C. E. Wyman, B. E. Dale, R. T. Elander, M. T. Holtzapple, M. R. Ladisch and Y. Y. Lee, *Bioresour. Technol.*, 2005, **96**, 1959–1966.
13 F. Teymouri, L. Laureano-Perez, H. Alizadeh and B. E. Dale, *Bioresour. Technol.*, 2005, **96**, 2014–2018.
14 M. W. Lau and B. E. Dale, *Proc. Natl. Acad. Sci. U. S. A.*, 2009, **106**, 1368–1373.
15 L. Laureano-Perez, F. Teymouri, H. Alizadeh and B. Dale, *Appl. Biochem. Biotechnol.*, 2005, **124**, 1081–1099.
16 P. Sarkar, E. Bosneaga and M. Auer, *J. Exp. Bot.*, 2009, **60**, 3615–3635.
17 J. Nakashima, T. Mizuno, K. Takabe, M. Fujita and H. Saiki, *Plant Cell Physiol.*, 1997, **38**, 818–827.
18 C. Somerville, S. Bauer, G. Brininstool, M. Facette, T. Hamann, J. Milne, E. Osborne, A. Paredez, S. Persson, T. Raab, S. Vorwerk and H. Youngs, *Science*, 2004, **306**, 2206–2211.
19 DuPont-Danisco, 2010, DuPont Danisco Cellulosic Ethanol (DDCE) and University of Tennessee/Genera Energy to hold grand opening for demonstration plant in Vonore, http://www.ddce.com/media/100107.html.
20 C. E. Wyman, B. E. Dale, R. T. Elander, M. T. Holtzapple, M. R. Ladisch and Y. Y. Lee, *Bioresour. Technol.*, 2005, **96**, 2026–2032.
21 T. H. Kim and Y. Y. Lee, *Bioresour. Technol.*, 2005, **96**, 2007–2013.
22 K. Öhgren, R. Bura, J. Saddler and G. Zacchi, *Bioresour. Technol.*, 2007, **98**, 2503–2510.
23 S. Kim and M. T. Holtzapple, *Bioresour. Technol.*, 2005, **96**, 1994–2006.
24 S. Kim and M. T. Holtzapple, *Bioresour. Technol.*, 2006, **97**, 778–785.
25 N. Mosier, R. Hendrickson, N. Ho, M. Sedlak and M. R. Ladisch, *Bioresour. Technol.*, 2005, **96**, 1986–1993.
26 S. Viamajala, M. Selig, T. Vinzant, M. Tucker, M. Himmel, J. McMillan and S. Decker, *Appl. Biochem. Biotechnol.*, 2006, **130**, 509–527.
27 S. Ding and M. Himmel, *J. Agric. Food Chem.*, 2006, **54**, 597–606.
28 J. Fahlen and L. Salmen, *J. Mater. Sci.*, 2003, **38**, 119–126.
29 T. Zimmermann, V. Thommen, P. Reimann and H. Hug, *J. Struct. Biol.*, 2006, **156**, 363–369.
30 M. Selig, S. Viamajala, S. Decker, M. Tucker, M. Himmel and T. Vinzant, *Biotechnol. Prog.*, 2007, **23**, 1333–1339.
31 J. Kristensen, L. Thygesen, C. Felby, H. Jørgensen and T. Elder, *Biotechnol. Biofuels*, 2008, **1**, 5.
32 S. G. Wi, A. P. Singh, K. H. Le and Y. S. Kim, *Ann. Bot. (Oxford, U. K.)*, 2005, **95**, 863–868.
33 A. Singh, G. Daniel and T. Nilsson, *J. Wood Sci.*, 2002, **48**, 95–98.
34 E. Crow and R. J. Murphy, *Bot. J. Linn. Soc.*, 2000, **134**, 339–359.
35 I. Boukari, J.-L. Putaux, B. Cathala, A. Barakat, B. Saake, C. Reìmond, M. O'Donohue and B. Chabbert, *Biomacromolecules*, 2009, **10**, 2489–2498.
36 Y. Uraki, Y. Usukura, T. Kishimoto and M. Ubukata, *Holzforschung*, 2006, **60**, 659–664.
37 S. V. Pingali, V. S. Urban, W. T. Heller, J. McGaughey, H. O'Neill, M. Foston, D. A. Myles, A. Ragauskas and B. R. Evans, *Biomacromolecules*, 2010, **11**, 2329–2335.
38 J. Kremer, D. Mastronarde and J. McIntosh, *J. Struct. Biol.*, 1996, **116**, 71–76.
39 P. Xu, L. Donaldson, Z. Gergely and L. Staehelin, *Wood Sci. Technol.*, 2007, **41**, 101–116.
40 D. N. Mastronarde, *J. Struct. Biol.*, 1997, **120**, 343–352.
41 N. Carpita, D. Sabularse, D. Montezinos and D. Delmer, *Science*, 1979, **205**, 1144–1147.
42 R. Chandra, R. Bura, W. Mabee, A. Berlin, X. Pan and J. Saddler, *Adv. Biochem. Eng./Biotechnol.*, 2007, **108**, 67–93.
43 R. P. Chandra, A. R. Esteghlalian and J. N. Saddler, in *Characterization of Lignocellulosic Materials*, ed. T. Hu, Blackwell, Oxford, UK, 2008, pp. 60–80.
44 S. J. Gregg and K. S. W. Sing, *Adsorption, Surface Area and Porosity*, Academic Press, London, 1982.
45 B. Buchanan, W. Gruissem and R. Jones, *Biochemistry and Molecular Biology of Plants*, Courier Companies Inc., 2001.
46 M. C. McCann, B. Wells and K. Roberts, *J. Cell Sci.*, 1990, **96**, 323–334.
47 J. Hafren, T. Fujino, T. Itoh, U. Westermark and N. Terashima, *Holzforschung*, 2005, **54**, 234–240.
48 M. Lau, C. Gunawan and B. Dale, *Biotechnol. Biofuels*, 2009, **2**, 30.
49 J. Bludworth and F. Carl Knopf, *J. Supercrit. Fluids*, 1993, **6**, 249–254.

This journal is © The Royal Society of Chemistry 2011

Energy Environ. Sci., 2011, **4**, 973–984 | 983

50 S. Chundawat, V. Balan and B. Dale, *Biotechnol. Bioeng.*, 2006, **96**, 219–231.
51 E. Sendich, M. Laser, S. Kim, H. Alizadeh, L. Laureano-Perez, B. Dale and L. Lynd, *Bioresour. Technol.*, 2008, **99**, 8429–8435.
52 T. Eggeman and R. T. Elander, *Bioresour. Technol.*, 2005, **96**, 2019–2025.
53 B. Bals, C. Wedding, V. Balan, E. Sendich and B. Dale, *Bioresour. Technol.*, 2010, DOI: 10.1016/j.biortech.2010.08.058, in press.
54 J. O'Connor, *Tappi*, 1972, **55**, 353–358.
55 P. Weimer, Y. Chou, W. Weston and D. Chase, *Biotechnol. Bioeng. Symp.*, 1986, **17**, 5–18.
56 B. S. Donohoe, M. J. Selig, S. Viamajala, T. B. Vinzant, W. S. Adney and M. E. Himmel, *Biotechnol. Bioeng.*, 2009, **103**, 480–489.
57 J. Fahlen and L. Salmen, *Biomacromolecules*, 2004, **6**, 433–438.
58 J. H. Grabber, R. D. Hatfield, F. Lu and J. Ralph, *Biomacromolecules*, 2008, **9**, 2510–2516.
59 J. Ralph, *Phytochem. Rev.*, 2010, **9**, 65–83.
60 M. Wada, Y. Nishiyama and P. Langan, *Macromolecules*, 2006, **39**, 2947–2952.
61 S. Chundawat, PhD dissertation, Michigan State University, 2009.
62 K. Igarashi, M. Wada and M. Samejima, *FEBS J.*, 2007, **274**, 1785–1792.
63 L. McCartney, S. E. Marcus and J. P. Knox, *J. Histochem. Cytochem.*, 2005, **53**, 543–546.
64 R. Atalla and D. Vanderhart, presented in part at the Institute for Paper Chemistry (IPC Technical Paper Series 217), 1987.
65 J. Ralph, R. D. Hatfield, S. Quideau, R. F. Helm, J. H. Grabber and H.-J. G. Jung, *J. Am. Chem. Soc.*, 1994, **116**, 9448–9456.
66 H. Kim and J. Ralph, *Org. Biomol. Chem.*, 2010, **8**, 576–591.
67 H. D. Graham, *J. Agric. Food Chem.*, 1992, **40**, 801–805.
68 D. Gao, S. P. S. Chundawat, C. Krishnan, V. Balan and B. E. Dale, *Bioresour. Technol.*, 2010, **101**, 2770–2781.
69 S. P. S. Chundawat, V. Balan and B. E. Dale, *Biotechnol. Bioeng.*, 2008, **99**, 1281–1294.